Hindawi
International Journal of Antennas and Propagation
Volume 2023, Article ID 8624191, 7 pages
https://doi.org/10.1155/2023/8624191

Research Article

Broadband Linear to Circular Polarizer Based on Multilayer Frequency-Selective Surface

Yi Yuan, Jun Ding, Chao Huang, Xia Ma, Xun Qu, and Chenjiang Guo

School of Electronics and Information, Northwestern Polytechnical University, Xi'an 710072, China

Correspondence should be addressed to Yi Yuan; yuanyi@mail.nwpu.edu.cn

Received 7 December 2022; Revised 23 February 2023; Accepted 9 March 2023; Published 21 March 2023

Academic Editor: Ashish Gupta

In this work, a transmission polarizer is described by using a frequency-selective surface to transform linearly polarized waves into circularly polarized waves. The linear to circular (LTC) polarizer consists of four layers. Two types of unit cells are designed in the LTC polarizer to improve design freedom. As a result, two orthogonal polarized components of transmission waves display nearly 90° phase differences while maintaining nearly high transparency for the generation of CPWs. The less than 3 dB axial ratio with a fractional width of over 76.8% from 9.20 to 20.67 GHz for this LTC polarizer is obtained. Even when the incident angle reaches 20°, its operating frequency band covers 9.69 to 20.21 GHz. Compared with the converters proposed before, the one proposed in this paper has a wider bandwidth. In order to evaluate the design strategy, a prototype is manufactured and tested. The results of the simulation and the experiment are in good accord.

1. Introduction

On the one hand, circularly polarized waves (CPWs) can reduce fading that is attributed to multipath scattering. On the other hand, a rotation of the electric field vector of linearly polarized waves may lead to degradation in the link budget, while CPWs do not have this problem. Therefore, CPWs are of essence for the wireless and satellite communication systems. Utilizing the radiators with non-canonical shapes [1] or unique feed arrangements, such as using a circularly polarized waveguide as the feed, which ensures the required conditions can be satisfied, is the traditional technique [2] for achieving CPWs. However, this way frequently results in design complexity and has a limited bandwidth due to the cutoff frequency of the waveguide. Another way to generate CPWs is to combine a linearly polarized antenna with a polarizer. The combination of the wideband antenna and the wideband polarizer can greatly expand the bandwidth. Therefore, the design of the wideband LTC polarizer is crucial in wireless and satellite communications.

Recently, metasurfaces have been widely used in various applications, including anomalous refraction and reflection [3–5], focusing lenses [6], polarization manipulation [7–16], the propagation of wave-to-surface wave coupling [17, 18], as well as the reduction of radar cross-sections [19–21], among many others [22–27]. Frequency-selective surface (FSS) is a significant type of metasurface that offers benefits for the LTC polarizer. For one component, the FSS can exhibit inductance characteristics, and for the other, it exhibits inductance characteristics. As a result, the transmitted wave has a phase difference between its two polarized components. Cascading the FSS can boost the transmission coefficient magnitude and bandwidth of the LTC polarizer. There have been numerous designs of LTC polarizers reported in the literature. In recent years, researchers have conducted extensive studies of LTC polarizers and obtained fruitful achievements. In [13], the researchers integrated the common dipole and square ring-basedband-pass FSS while modifying the dimensions of the FSS structure to control the high-efficiency pass bands and transmission phases for two orthogonal polarizations; an axial ratio of less than 3 dB was obtained, with a bandwidth of about 23.8%.

By utilizing multiple cascaded FSS layers, we propose a novel wideband LTC polarizer. Some previous literature has mentioned the idea of exploiting multiple cascaded

layers in LTC polarizers [11–13, 15, 16]. However, these solutions adopt the same cascading layers, which are characterized by high insertion loss (IL), low design freedom, and narrow bandwidth. In view of the above limitation, we propose an LTC polarizer that offers a wide operating frequency range with low IL and high design freedom. The paper is structured as follows: in Section 2, the LTC polarizer in this paper is designed and the equivalent circuit model is analyzed. In Section 3, we discuss the manufactured prototype and measurements. Finally, the conclusion is described in Section 4.

2. Analysis and Design of the Proposed LTC Polarization

As shown in Figures 1(a) and 1(b), the proposed LTC polarizer consists of two different types of unit cells. The split square ring and metal wire in the center make up the top and bottom layers. The two middle layers consist of a wire and four square patches. The wire in the top and bottom layers is identical to the wire in the middle layers. The unit cell of each layer has a period of a. For the split square ring unit cell, l_1 represents the length of the split square ring, and w_1 is the width of the split square ring. g_1 and g_2 represent the gap of the split square ring in the x and y directions, respectively. For the square patches unit cell, l_2 and w_2 are the length and width of the square patches, respectively. The four square patches have the same dimension. g_3 represents the distance of the patches in the x direction, and g_4 is the distance of the patches in the y direction. The width of the metal wire is w. The structure is printed on the F4B dielectric substrate with the $\varepsilon_r = 2.2$ and the thickness is h.

Figure 1(c) shows the structure of the four layers of the LTC polarizer. The distance between each layer is t. The two outer layers adopt the same split square ring, and the two inner layers adopt the same square patches. It is worth noting that for both the split square ring and square patches unit cells, due to the presence of the metal wire, they show asymmetric structures in the x and y directions. The asymmetric structures of the unit cell make the phase difference between the x and y polarizations possible. It is well known that an incident wave polarized 45° from the x-axis can be decomposed into two waves with x and y polarizations, $\mathbf{E}_{\mathbf{x}}^{(\mathbf{i})}$ and $\mathbf{E}_{\mathbf{y}}^{(\mathbf{i})}$, that are equal in magnitude and phase. A wave of this type can be represented as

$$\mathbf{E}^{(\mathbf{i})} = \mathbf{E}_{\mathbf{x}}^{(\mathbf{i})} + \mathbf{E}_{\mathbf{y}}^{(\mathbf{i})} = \mathrm{E}_0\left(\mathbf{a}_{\mathbf{x}} + \mathbf{a}_{\mathbf{y}}\right)\mathrm{e}^{\mathrm{jkz}}, \tag{1}$$

where a_x is the unit vector in the x direction, a_y is the one in the y direction, E_0 is the amplitude of the incident wave, and k is the wave number.

Then, the transmitted wave after such incident wave passes through the surface can be expressed as

$$\begin{aligned} \mathbf{E}^{(\mathbf{t})} = \mathbf{E}_{\mathbf{x}}^{(\mathbf{t})} + \mathbf{E}_{\mathbf{y}}^{(\mathbf{t})} = \mathrm{E}_0\left(\mathbf{T}_{\mathbf{xx}}\mathbf{a}_{\mathbf{x}} + \mathbf{T}_{\mathbf{yy}}\mathbf{a}_{\mathbf{y}}\right)\mathrm{e}^{\mathrm{jkz}}, \\ \mathbf{T}_{\mathbf{xx}} = \mathrm{T}_{\mathrm{xx}}\mathrm{e}^{\mathrm{j}\varphi_{\mathrm{xx}}}, \mathbf{T}_{\mathbf{yy}} = \mathrm{T}_{\mathrm{yy}}\mathrm{e}^{\mathrm{j}\varphi_{\mathrm{yy}}}, \end{aligned} \tag{2}$$

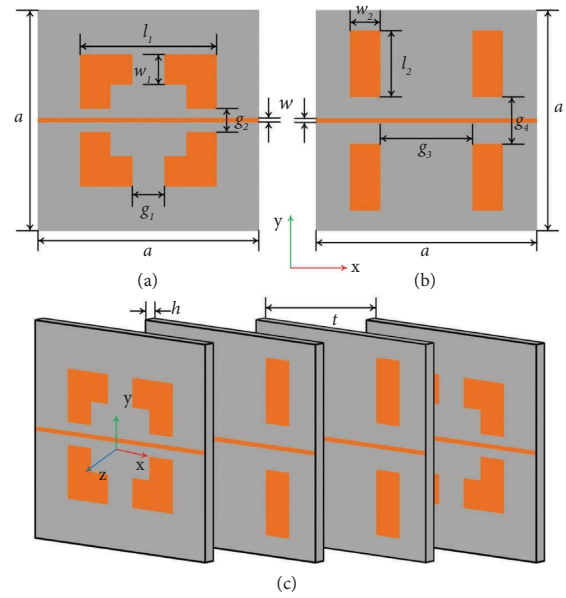

Figure 1: The structures of (a) the split square ring, (b) the square patches unit cell, and (c) the LTC polarizer.

where T_{xx} and φ_{xx} are the transmission coefficient magnitude and phase in the x direction and T_{yy} and φ_{yy} are the ones in the y direction. The conditions for generating CPWs are as follows:

$$\begin{aligned} T_{xx} &= T_{yy}, \\ \Delta\varphi &= \varphi_{xx} - \varphi_{yy} = 90^{\circ}. \end{aligned} \tag{3}$$

When the conditions are met, the incident wave polarized 45° from the x-axis can be converted to a CPW. As shown in Figure 2, the equivalent circuits of the proposed LTC polarizer are described. By controlling the width and distance of the metal wire, the value of the inductance and capacitance can be controlled independently. The main property of the spilt square ring resonator is the resonant behavior of its reflection coefficient. This resonant reflection occurs when the circumference of the ring is approximately equal to the wavelength. For the split square ring unit cell, the split square ring is equivalent to a series resonant circuit $L_1 - C_1$. Because the structure of the split square ring is symmetric, the capacitance C_1 and inductance L_1 are equal in the x and y directions. C_x and C_y represent the coupling capacitance between the unit cells in the x and y directions. The inductance will be generated in the x direction due to the metal wire. Thus, the structure is inductive in the x direction and capacitive in the y direction. This results in a phase difference in the x and y directions. By adjusting the distance of the gap and the width of the metal wire, the transmission band and phase difference in the x and y directions can be changed. For the square patches unit cell, the square patches produce capacitance C_2 and C_3 in the x and y directions, respectively. The length and width of the patches can be changed to alter the coupling capacitance in both directions. In the x direction, the metal wire and square patches are equivalent to a parallel resonant circuit $L_3 - C_3$,

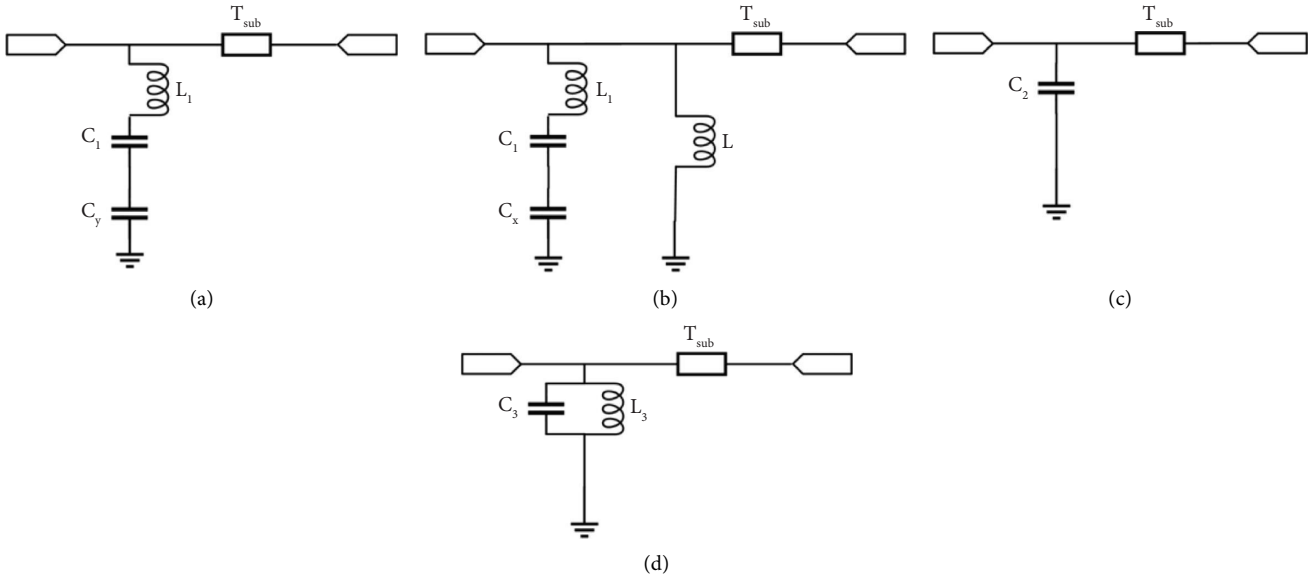

FIGURE 2: The equivalent circuit models of the polarizer. (a) The split square ring unit cell in the y direction for y polarization. (b) The split square ring unit cell in the y direction for x polarization. (c) The square patches unit cell in the x direction for y polarization. (d) The square patches unit cell in the x direction for x polarization.

while in the y direction, only capacitance is present. Additionally, the structure is capacitive in the y direction and inductive in the x direction. By changing the size of the patch and the width of the wire, the capacitance value and the inductance value can be adjusted to control the resonant frequency. For the two different unit cells, the introduction of split square ring and square patches provides greater freedom for the design of the LTC polarizer. The introduction of the multilayer structure makes the polarizer generate multiple resonant frequency, thus broadening the bandwidth of the polarizer. The dielectric substrate is modeled as T_{sub} using a transmission line. The air space on both sides of each layer is modeled with a transmission line as a characteristic impedance $\eta = 377\Omega$.

The equivalent circuit model was used to design the original LTC polarizer. The subsequent optimization of the structural parameters is carried out in ANSYS HFSS. The periodic boundary condition is used to simulate the infinite period array along the x and y directions, and the Floquet port is used to simulate the x-and y-polarized wave incident in the z direction. The structural parameters of the proposed LTC polarizer are shown below: $a = 11$ mm, $l_1 = 6.6$ mm, $l_2 = 3.3$ mm, $w = 0.2$ mm, $w_1 = 1.5$ mm, $w_2 = 1.5$ mm, $g_1 = 1.5$ mm, $g_2 = 1.1$ mm, $g_3 = 4.6$ mm, $g_4 = 1.1$ mm, $h = 0.381$ mm, and $t = 5.5$ mm.

Figure 3(a) presents the simulated results, containing transmission coefficient magnitudes $|\mathbf{T_{xx}}|$ and $|\mathbf{T_{yy}}|$, transmission phases φ_{xx} and φ_{yy}, and the phase difference $\Delta\varphi$. A transmission coefficient magnitude better than 0.9 has a bandwidth of about 70.2% between 8.88 and 18.49 GHz. The bandwidth of the phase difference $\Delta\varphi$ about 90° is from 10.80 to 20.64 GHz.

The axial ratio (AR) for this LTC polarizer can be determined as

$$\mathrm{AR} = \left(\frac{|\mathbf{T_{xx}}|^2 + |\mathbf{T_{yy}}|^2 + \sqrt{\mathrm{a}}}{|\mathbf{T_{xx}}|^2 + |\mathbf{T_{yy}}|^2 - \sqrt{\mathrm{a}}} \right)^{1/2} \tag{4}$$

$$\mathrm{a} = |\mathbf{T_{xx}}|^4 + |\mathbf{T_{yy}}|^4 + 2|\mathbf{T_{xx}}|^2 |\mathbf{T_{yy}}|^2 \cos(2\Delta\varphi).$$

The simulated AR value of the different layers is shown in Figure 3(b). As shown in Figure 3(b), there is a less than 3 dB axial ratio over 76.8% from 9.20 to 20.67 GHz for the LTC polarizer. By comparing the AR values of different layers, although the AR values of three and four layers are less than 3 dB, the AR value of four layers is obviously better than that of three layers within the operating bandwidth. The transmission field may be combined to express the left-hand circularly polarized (LHCP) and right-hand circularly polarized (RHCP) wave components. Figure 4(a) shows the LTC polarization transmission results. It can be concluded that the proposed LTC polarizer has low cross-polarization.

The performance of the LTC polarizer is directly connected to variations in incident angle for the periodic structure. The simulated AR value of several incident angles is shown in Figure 4(b). The simulated AR bandwidth is comparatively steady when θ is varied from 0° to 20°, staying under 3 dB from 9.69 to 20.21 GHz. When θ is varied from 20° to 30°, the bandwidth of the polarizer becomes narrow. When θ is greater than 30°, the performance of the polarizer deteriorates, especially at high frequencies. The values of various layer spacings t are then examined in order to comprehend the impact of assembly errors on the performance of the LTC polarizer. All other parameters remain constant when t changes.

The variation trend of $\beta = (|\mathbf{T_{xx}}|/|\mathbf{T_{yy}}|)$ and $\Delta\varphi$ for different t is shown in Figure 5(a). The bandwidth of $\Delta\varphi =$

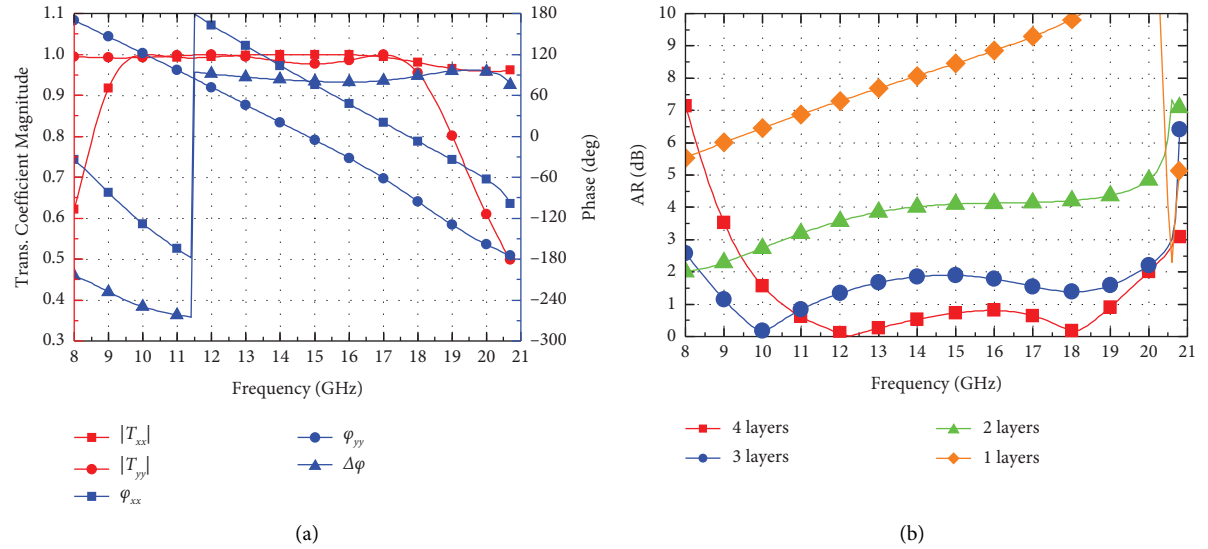

Figure 3: (a) Simulated transmission coefficient magnitude, transmission phase, and phase difference. (b) AR value for different layers.

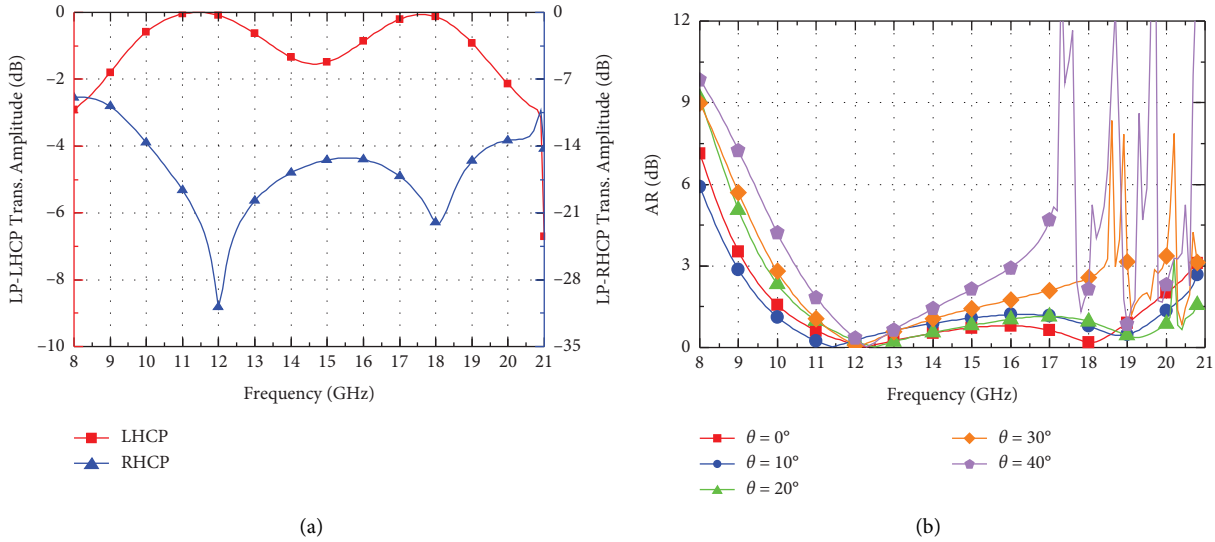

Figure 4: (a) Magnitudes of LHCP and RHCP. (b) AR value of different incident angle θ.

90° progressively moves to the left as t increases. The AR value for different t is shown in Figure 5(b). It shows that when t varies within a certain range, the proposed LTC polarizer can still obtain a good AR bandwidth in the operating frequency, which is beneficial to the manufacture and assembly of the polarizer.

3. Experimental Verification

To verify the performance of the wideband LTC polarizer, a prototype has been fabricated, as shown in Figure 6(a). The LTC polarizer contains 19 × 19 unit cells with dimensions of 209 × 209 × 16.5 mm. The cascade of the four FSS layers has been fixed by nylon screws. In Figure 6(b), two linear polarized horn antennas are linked to a vector network analyzer. Then, the performance of the LTC polarizer is measured.

Figures 7(a) and 7(b) show the comparison of the magnitudes of the simulated and measured transmission coefficient magnitudes as well as the transmission phase difference between x-polarization and y-polarization. The AR value can be determined using the measurement results by using equation (4), as shown in Figure 8. Thus, the conclusion is that measured transmission magnitudes, phase difference, and AR values are consistent with simulated ones in general. There are two main factors for the slight differences. In one instance, a small distance during the test will change the phase, while in another instance, the tolerance employed in fabrication and assembly will cause the difference.

In the end, the key results of the proposed wideband LTC polarizer are concluded in Table 1. As shown in Table 1, compared to the LTC polarizer presented in previous literature, the LTC polarizer in the paper has a broader

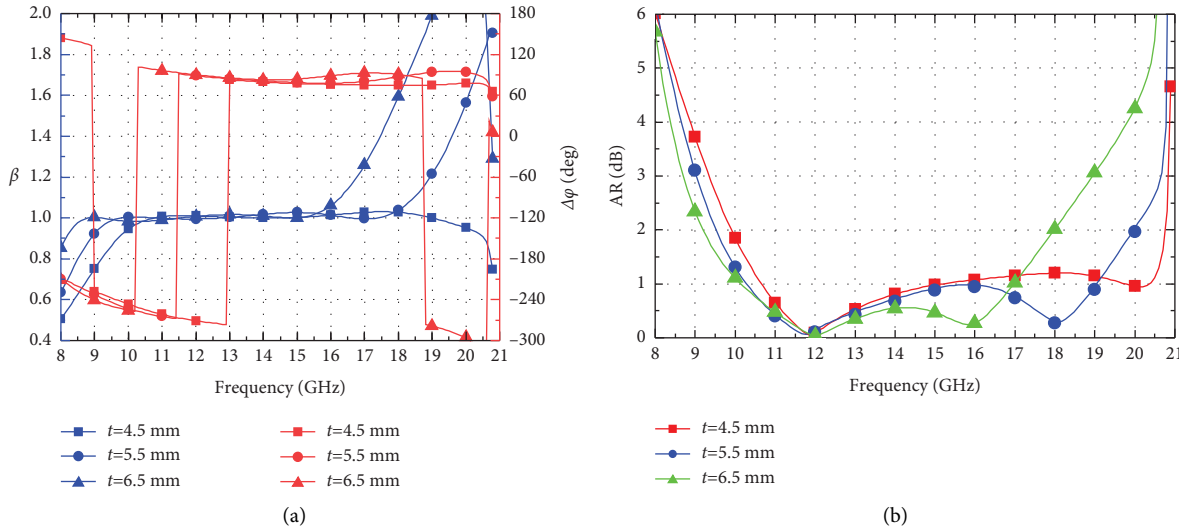

(a) (b)

Figure 5: (a) The variation trend of β and $\Delta\varphi$ with the different t. (b) AR value for different t.

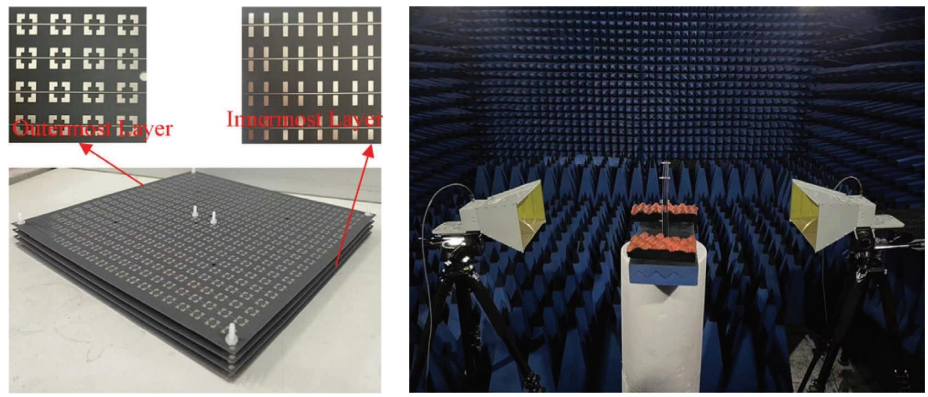

(a) (b)

Figure 6: (a) LTC polarizer manufactured prototype. (b) The measurement setup.

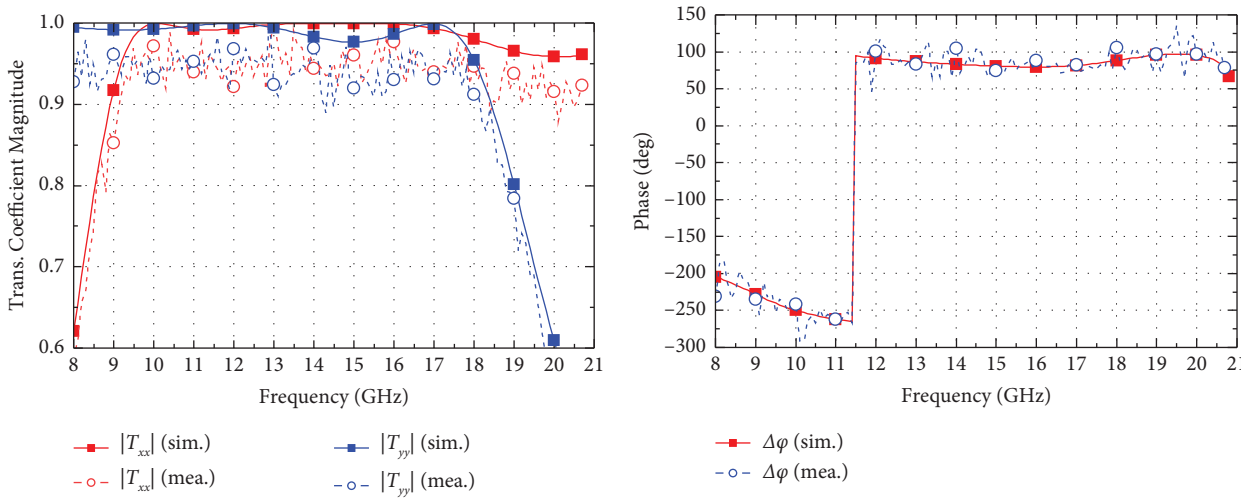

(a) (b)

Figure 7: Measured (a) transmission coefficient magnitudes and (b) phase difference.

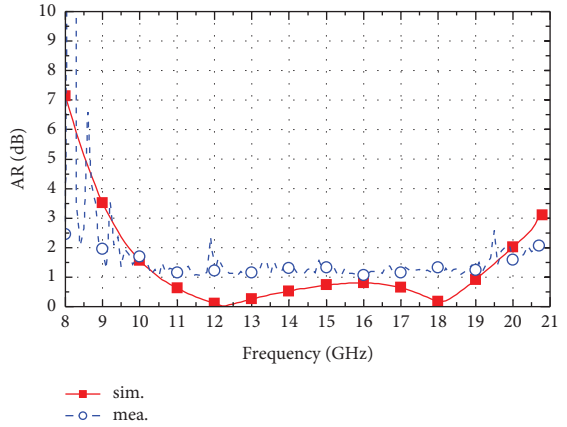

Figure 8: Measured AR value.

Table 1: The key results of the proposed wideband LTC polarizer.

References	Layer	Unit size	Thickness	AR BW (%)	Max IL (dB)	Angular stability
[10]	1	$0.4\lambda_0$	$0.05\lambda_0$	31.8	3	*
[11]	2	$0.3\lambda_0$	$0.23\lambda_0$	20	1.79	±40°
[12]	2	$0.35\lambda_0$	$0.27\lambda_0$	24	1.1	±50°
[15]	5	$0.32\lambda_0$	$0.57\lambda_0$	19.6	1	±50°
[16]	3	$0.17\lambda_0$	$0.21\lambda_0$	11	0.4	±30°
This work	4	$0.51\lambda_0$	$0.79\lambda_0$	76.8	1	±20°

Note. *represents no mention.

bandwidth and lower IL. At the same time, due to the limitation of the thickness and the angle stability, the application of a polarizer in a compact system and a beam scanning antenna is limited.

4. Conclusions

A novel wideband LTC polarizer is proposed. Using a four-layer structure, the polarizer provides a wideband, high-efficiency transmission band. A transmission coefficient magnitude better than 0.9 has a bandwidth of about 70.2% between 8.88 and 18.49 GHz. There is a less than 3 dB axial ratio over 76.8% from 9.20 to 20.67 GHz for this polarizer. The operating frequency range of the polarizer remains 9.69 to 20.21 GHz even when the incident angle is increased to 20°. Besides being simple to construct and assemble, the wideband LTC polarizer proposed in this paper is also inexpensive and has a wide range of practical applications.

Data Availability

The structure parameter data used to support the findings of this study are included within the article.

Conflicts of Interest

The authors declare that there are no conflicts of interest regarding the publication of this paper.

References

[1] H. L. Zhu, S. W. Cheung, H. X. Liu, and T. I. Yuk, "Design of polarization reconfigurable antenna using metasurface," *IEEE Transactions on Antennas and Propagation*, vol. 62, no. 6, pp. 2891–2898, 2014.

[2] X. T. Son and I. Park, "Compact wideband circularly polarized patch antenna array using metasurface," *IEEE Antennas and Wireless Propagation Letters*, vol. 16, pp. 1932–1936, 2017.

[3] H. Kim and S. Nam, "Performance improvement of LC-basedbeam-steeringleaky-wave holographic antenna using decoupling structure," *IEEE Transactions on Antennas and Propagation*, vol. 70, no. 4, pp. 2431–2438, 2022.

[4] J. Luo, L. Li, J. Su, R. Ma, and S. Han, "Multibeam antenna based on partially reflecting defected metasurface," *IEEE Antennas and Wireless Propagation Letters*, vol. 20, no. 8, pp. 1582–1586, 2021.

[5] X. Ding, F. Monticone, K. Zhang, L. Zhang, and D. Gao, "Ultrathin pancharatnam-berry metasurface with maximal cross-polarization efficiency," *Advanced Materials*, vol. 27, no. 7, pp. 1195–1200, 2015.

[6] L. Qun and N. C. Zhi, "Flat-focal-planedual-metasurface lens for low scan loss and sidelobe level of a metalens antenna," *IEEE Transactions on Antennas and Propagation*, vol. 70, no. 10, pp. 9849–9854, 2022.

[7] C. Yang, X. W. Zhu, P. Liu, and W. Hong, "A circularly polarized horn antenna based on an FSS polarization converter," *IEEE Antennas and Wireless Propagation Letters*, vol. 19, no. 2, pp. 277–281, 2020.

[8] M. A. Sofi, K. Saurav, and S. K. Koul, "A linear to circular polarization reconfigurable converter based on frequency selective surface," *Microwave and Optical Technology Letters*, vol. 63, no. 5, pp. 1425–1433, 2021.

[9] S. Clendinning, R. Cahill, D. Zelenchuk, and V. Fusco, "Influence of dielectric layers on performance of transmission mode frequency selective surface based linear to circular polarization transformers," *Microwave and Optical Technology Letters*, vol. 62, no. 4, pp. 1815–1823, 2020.

[10] L. Yuan, L. Hou, and Z. Yang, "Triple-bandultra-thin linear to circular polarization converter based on transmission metasurface," *Microwave and Optical Technology Letters*, vol. 64, no. 1, pp. 54–59, 2022.

[11] F. Alessio Dicandia and S. Genovesi, "Linear-to-Circular polarization transmission converter exploiting meandered metallic slots," *IEEE Antennas and Wireless Propagation Letters*, vol. 21, no. 11, pp. 2191–2195, 2022.

[12] E. Arnieri, F. Greco, and G. Amendola, "A broadband, wide-angle scanning, linear-to-circular polarization converter based on standard jerusalem cross frequency selective surfaces," *IEEE Transactions on Antennas and Propagation*, vol. 69, no. 1, pp. 578–583, 2021.

[13] Z. Wang, Y. Ge, C. Lin, and K. Liu, "High-efficiency cross and linear-to-circular polarization converters based on novel frequency selective surfaces," *Microwave and Optical Technology Letters*, vol. 61, no. 10, pp. 2410–2419, 2019.

[14] M. Xie, B. Li, and L. Zhu, "Dual-band circular polarizers with versatile polarization conversions based on aperture-coupled patch resonators," *IEEE Transactions on Antennas and Propagation*, vol. 70, no. 7, pp. 5584–5596, 2022.

[15] D. Blanco and R. Sauleau, "Broadband and broad-angle multilayer polarizer based on hybrid optimization algorithm for low-costka-band applications," *IEEE Transactions on Antennas and Propagation*, vol. 66, no. 4, pp. 1874–81, 2018.

[16] M. Hosseini and S. V. Hum, "A circuit-driven design methodology for a circular polarizer based on modified jerusalem cross grids," *IEEE Transactions on Antennas and Propagation*, vol. 65, no. 10, pp. 5322–5331, 2017.

[17] S. Sun, Q. He, S. Xiao, Q. Xu, and X. Li, "Gradient-indexmetasurfaces as a bridge linking propagating waves and surface waves," *Nature Materials*, vol. 11, no. 5, pp. 426–431, 2012.

[18] C. Wu, Y. Cheng, W. Wang, and B. He, "Ultra-thin and polarization-independent phase gradient metasurface for high-efficiency spoof surface-plasmon-polariton coupling," *Applied Physics Express*, vol. 8, no. 12, pp. 8–12, 2015.

[19] S. Deng, X. Zhang, J. Ding, H. Zhang, and W. Chen, "Low-profilehigh-gain broadband circularly polarized slot antenna with RCS reduction using polarization conversion metasurface," *Microwave and Optical Technology Letters*, vol. 65, no. 1, pp. 281–289, 2022.

[20] Y. Liu, Y. Jia, W. Zhang, and F. Li, "Wideband RCS reduction of a slot array antenna using a hybrid metasurface," *IEEE Transactions on Antennas and Propagation*, vol. 68, no. 5, pp. 3644–3652, 2020.

[21] X. Liu, J. Gao, L. Xu, X. Cao, and Y. Zhao, "A coding diffuse metasurface for RCS reduction," *IEEE Antennas and Wireless Propagation Letters*, vol. 16, pp. 724–727, 2017.

[22] L. Liu, X. Zhang, M. Kenney, X. Su, and N. Xu, "Broadband metasurfaces with simultaneous control of phase and amplitude," *Advanced Materials*, vol. 26, no. 29, pp. 5031–5036, 2014.

[23] K. Chen, Y. Feng, F. Monticone, J. Zhao, and B. Zhu, "A reconfigurable active huygens' metalens," *Advanced Materials*, vol. 29, no. 17, pp. 1–7, 2017.

[24] M. Khorasaninejad, W. Cheng, R. C. Devlin, and J. OH, "Metalenses at visible wavelengths: diffraction-limited focusing and subwavelength resolution imaging," *Science*, vol. 352, no. 6290, pp. 1190–1194, 2016.

[25] K. Katoch, N. Jaglan, and S. D. Gupta, "Design and analysis of single sided modified square loop UWB frequency selective surface," *IEEE Transactions on Electromagnetic Compatibility*, vol. 63, no. 5, pp. 1423–1432, 2021.

[26] K. Katoch, N. Jaglan, S. D. Gupta, and M. S. Sharawi, "Design of a triple band notched polarization independent compact FSS at UWB frequency range," *International Journal of RF and Microwave Computer-Aided Engineering*, vol. 31, no. 6, Article ID e22631, 2021.

[27] K. Katoch, N. Jaglan, and S. D. Gupta, "Analysis and design of a simple and compact bandstop frequency selective surface at mobile WiMAX and satellite communication X-band," *Journal of Electromagnetic Waves and Applications*, vol. 35, no. 10, pp. 1321–1336, 2021.